

# Is There a Disc in the Superluminal Quasars?

E. Rokaki,<sup>1,2,3</sup> A. Lawrence,<sup>2,3</sup> F. Economou<sup>3,4</sup> & A. Mastichiadis<sup>1</sup>

<sup>1</sup> *Section of Astrophysics, Astronomy & Mechanics, University of Athens, 15784 Zografos, Athens, Greece*

<sup>2</sup> *Institute for Astronomy, University of Edinburgh, Royal Observatory, Blackford Hill, Edinburgh, UK*

<sup>3</sup> *Physics Department, Queen Mary and Westfield College, Mile End Road London E1 4NS, UK*

<sup>4</sup> *UKIRT, JACH, Hawaii*

## ABSTRACT

We look for the expected signature of an accretion disc by examining the properties of the  $H\alpha$  emission line versus viewing angle in a sample of 22 superluminal (SL) quasars. The Doppler factor  $\delta$ , jet velocity  $\gamma$ , and viewing angle towards the jet  $\theta$ , are derived from published radio and X-ray data. Most of the  $H\alpha$  spectra (fourteen) have been observed at the United Kingdom Infrared Telescope (*UKIRT*) and are reported here. About one fourth of the SL objects have weak or absent  $H\alpha$  emission lines, with small equivalent widths (EW). These have high optical polarization, radio core dominance, Doppler factor and most of them high apparent SL velocity and low viewing angles. Therefore these weak-EW objects almost certainly have relativistically beamed optical continua. The strong-EW objects also show a clear beaming effect, but a much weaker one, with line EW varying by only a factor three while radio core dominance varies by a factor of several hundred. The correlation of EW with  $\theta$  is quantitatively in good agreement with the prediction of a flat accretion disc with limb darkening. The weak- and strong-EW sources also show an anti-correlation of line velocity width with the various beaming indicators. Again, the correlation with the derived viewing angle  $\theta$  shows a quantitative agreement with the effect expected for an axisymmetric structure with velocity dominated by rotation. The line emission cannot come from the surface of the disc, or the line beaming would cancel the continuum beaming. However it could come from an axisymmetric system of clouds co-rotating with the accretion disc.

**Key words:** galaxies: active - quasar: emission lines - quasars: general - radio continuum: galaxies - accretion disc

## 1 INTRODUCTION

Attempts to incorporate all AGN (active galactic nuclei) activity within some framework (“Unified Schemes”) have focused on the importance of the orientation of the observer with respect to the source, in three separate ways. (i) The most dramatic effect is relativistic Doppler-beaming in a jet of radio-emitting plasma aligned close to the line of sight. Amplification of the apparent brightness of the source and apparent superluminal motions are then expected (Rees 1966; Lind & Blandford 1985; Ghisellini *et al.* 1993; Urry & Padovani 1995). This effect explains the existence of “blazars”, objects dominated by a polarised and highly variable continuum, as well as one sided radio jets and other phenomena. This is the most well established orientation effect, but only applies to the minority of radio-loud objects. (ii) The second effect is that of absorption or obscuration, most probably by an equatorial disc or torus, invoked to account for the dissimilarities between type 1 and type 2 Seyfert galaxies (Lawrence & Elvis 1982, Antonucci & Miller

1985, Antonucci 1993). (iii) Finally a third orientation effect is associated with an accretion disc geometry: (a) a simple optically thick, geometrically thin disc viewed inclined will appear fainter than when it is viewed pole on. However relativistic effects in the vicinity of the accreting black hole make edge-on discs brighter (Cunningham 1975). (b) If the emission lines share the same geometry they will have a broad velocity width at low latitude. (c) The polarization of the disc radiation will increase with the inclination (e.g. Rees 1975).

Some authors have searched for evidence of this third class of orientation dependent effects, generally by using the ratio of core radio luminosity to extended radio luminosity (e.g. Orr & Browne 1982; Wills & Browne 1986; Browne & Murphy 1987; Jackson *et al.* 1989; Jackson & Browne 1991b; Corbin 1997). This ratio is an orientation indicator (see for instance Ghisellini *et al.* 1993, Wills & Brotherton 1995) and these studies have been consistent with the widespread presence of optical beaming in radio loud quasars in general (as opposed to simply in blazars, e.g. Browne & Murphy 1987)

and a flattened geometry for the emission lines (e.g. Wills & Browne 1986, Corbin 1997). The amount of optical beaming seen is far less than seen in the radio regime, indicating that it might be due to relativistic beamed continuum seen in low contrast against less anisotropic disc emission (e.g. Browne & Murphy 1987; Wills 1991; Wills *et al.* 1992). The idea of this paper is to use *superluminal sources* for which we can derive an actual viewing angle rather than an indirect orientation indicator, and so directly test for the *quantitative* effects of accretion disc surface brightness and emission line velocity projection (see also Wills & Brotherton 1995).

In this paper, we study the H $\alpha$  emission of a sample of 22 superluminal sources. This line was chosen because it is the strongest low ionization emission line (LIL, e.g. hydrogen Balmer, Mg II etc.) for which, there are both observational (e.g. Wills & Browne 1986) and theoretical (e.g. Collin-Souffrin 1987) suggestions that its velocity field is anisotropic, likely in a rotational disc structure. In addition, H $\alpha$  line is less affected by absorption or blended optical Fe II multiplet emission than H $\beta$ . Line width is used to study velocity projection, and equivalent width to indicate the brightness of the underlying continuum. The viewing angle is derived from published SL motions, radio and X-ray fluxes, and angular sizes, using the method of Ghisellini *et al.* (1993). For eight sources we use published H $\alpha$  data, but for the majority we have obtained new data. Most superluminal sources are at moderately large redshifts, so this has required obtaining IR spectra, which we report in this paper.

In Section 2 we summarise the technique used to derive viewing angle. In Section 3, we describe the SL sample giving relevant data and the parameters derived by the Inverse Compton model. In Section 4, we present the new *UKIRT* observations, with detailed source notes in Section 5. In Section 6 we present the statistical results which are discussed in Section 7 and summarised in Section 8. The cosmological model assumed in this paper is  $H_0 = 75 \text{ km s}^{-1} \text{ Mpc}^{-1}$  and  $q_0 = 0.5$ .

## 2 METHOD OF DERIVING VIEWING ANGLE

Derivation of the viewing angle relies on two effects - superluminal motion, and Doppler boosting. We follow the method of Ghisellini *et al.* (1993) which we now summarise briefly.

Apparent Super-Luminal (SL) motions of individual radio structures (measured with *VLBI* experiments, see for instance Zensus & Pearson 1987) have been observed in extragalactic radio sources for more than 20 years. These motions are usually modelled by one or more radiating “blobs” moving at relativistic velocity  $\beta$  (in units of  $c$ ) away from a stationary “core”. If the viewing angle is  $\theta$ , the apparent transverse velocity is

$$\beta_a = \frac{\beta \sin \theta}{1 - \beta \cos \theta} \quad (1)$$

and can exceed the true speed and even that of light if the direction of the motion is close to the line of sight. The observed SL velocity therefore gives a combination of the Lorentz factor  $\gamma$ , and jet viewing angle  $\theta$ . The radiating material is brightened by the Doppler beaming factor  $\delta$ , which also provides a combination of  $\gamma$  and  $\theta$  ( $\delta = [\gamma(1 - \beta \cos \theta)]^{-1}$ ). If  $\delta$  can be separately estimated, then, following Appendix B of Ghisellini *et al.* (1993),  $\gamma$  and  $\theta$  are given by

$$\gamma = \frac{\beta_a^2 + \delta^2 + 1}{2\delta} \quad (2)$$

and

$$\tan \theta = \frac{2\beta_a}{\beta_a^2 + \delta^2 - 1} \quad (3)$$

The value of  $\delta$  is estimated from observations of the flat spectrum radio core, assumed to be made up of multiple self-absorbed components, by requiring that the Inverse Compton flux of the component peaking at the observed radio frequency is less than the observed X-ray flux (see equation 1 of Ghisellini *et al.*). This also requires the angular size of the source, from *VLBI* measurements, and an assumption for the underlying synchrotron spectral slope, taken to be  $\alpha = 0.75$ .

We summarise uncertainties in the estimate of  $\theta$ . (i) The value of  $\delta$  estimated from the X-ray flux is a lower limit, and so the derived  $\theta$  is an upper limit. However the value is very insensitive to this effect -  $\delta \propto F_x^{-0.22}$ . So if the true  $F_x$  is actually lower by a factor 10, 100, or 1000, the value of  $\delta$  is larger by a factor 1.5, 2.3, and 3.5 respectively. This factor might increase by up to 30 % if the source is not spherical as assumed, but a continuous jet (see equation 2 of Ghisellini *et al.*) (ii) Radio flux and angular size errors may also introduce uncertainties on  $\theta$ , but in most cases these are not large. (iii) Another possibility is that the superluminal velocities represent a pattern velocity which is different than the bulk velocity (Lind & Blandford 1985; Vermeulen & Cohen 1994). (iv) Finally the observed value of  $\beta_a$  and thus  $\theta$  depends on the assumed Hubble constant, but we take that to be understood (Freedman *et al.* 2001). If  $H_0$  is smaller than the assumed value,  $\theta$  is smaller in most cases. In section 6 we provide arguments that  $\delta$  cannot be wrong by a very large factor, but also illustrate the effect on derived values of  $\theta$  of assuming that  $\delta$  is wrong by a factor of a few.

## 3 THE SAMPLE

The sample of the SL sources was selected from the list of Vermeulen & Cohen, 1994 (VC94). The final sample used in this paper is the superset of those for which we were able to obtain good quality IR spectra at *UKIRT*, plus those with published (optical) data on H $\alpha$ . This sample represents more than the one third of the known SL extragalactic sources. It is listed in Table 1. Columns (1), (2), (4), (5), and (6) list names, redshift, the fastest measured apparent velocity, and the core-to-lobe flux ratio  $R$  at 5 GHz

as given in VC94. Column (3) divides the objects into three classes depending on radio core dominance and optical polarization. Core dominated sources with low polarization are shown as “CD” and those with high polarization ( $P > 3\%$ ) as “CDP”. Lobe dominated sources are shown as “LD”. The limit between CD and LD was taken as  $\log R = -0.02$ .

Columns (7)-(10) give the observed radio core flux and angular size ( $\theta_d = \sqrt{ab}$  where  $a$  and  $b$  are the major and minor axes in mas) at a given frequency, together with the reference. Finally the two last columns give the observed X-ray flux at 1 keV together with the reference. The radio and X-ray data were then used to estimate  $\delta$ , and thus  $\theta$ , and  $\gamma$ , as explained in the section above. For 3C 395 we have not found any X-ray measurement published, and we have used optical data instead. Table 2 shows the result, with sources listed in order of increasing  $\theta$ , which can be seen to correlate clearly with  $\delta$  but not with  $\gamma$ , as expected in the beaming model.

## 4 UKIRT SPECTRA

### 4.1 Observations and Data reduction

From the VC94 sample only objects between RA  $05^h$  and  $19^h$  and Dec. lower than  $60^\circ$  were observed, due respectively to the time of year of the observations and the declination limit of the telescope. Finally we selected sources at redshifts that would place  $H\alpha$  well inside one of the  $J$ ,  $H$ , or  $K$  atmospheric windows. This gave 14 sources which are listed in Table 3. 3C 286 (not known as superluminal) was also observed during an RA gap in the run and is likewise listed in Table 3.

The spectra were obtained with the common-user Cooled Grating Spectrometer CGS4 at the  $f/36$  focus of the 3.9-m *UKIRT* on Mauna Kea, on three consecutive photometric nights starting on UT date 1994 March 27. The instrument was equipped at this time with a  $62 \times 58$  InSb array detector at the focal plane of a 150-mm camera with a slit of width equal to 3 arcsec, stepped perpendicular to the dispersion. The detector was stepped in increments of one-third of a resolution element in order to properly sample the instrumental profile. Different gratings and orders used, depending on the redshift of the source, and exposure times, are given in Table 3.

For most of the  $J$ - and  $H$ - band observations, a 75 line  $\text{mm}^{-1}$  grating in second order was used. This gave a resolving power of 383 and  $0.2 \mu\text{m}$  spectral coverage. For one case in the  $J$ - band, the 150 line  $\text{mm}^{-1}$  grating was used in third order, giving a resolving power of 1000 and a wavelength coverage  $0.1 \mu\text{m}$ . For observations in the  $K$ -band the 75  $\text{mm}^{-1}$  grating was used in first order, giving a resolving power of 337 and  $0.4 \mu\text{m}$  spectral coverage.

Standard nodding procedures were followed to subtract the sky background, with the slit oriented east-west on the sky. While observing, we nodded on to the detector so that

we could integrate on the object while obtaining frames for sky subtraction. Bias frames were subtracted and the observation images were then flat-fielded. An argon lamp and vacuum wavelengths are used here for the wavelength calibration. Correction for atmospheric extinction was applied by observing a spectral standard star at a similar airmass to the object. Flux calibration was achieved by extrapolating  $J$ ,  $H$  and  $K$  magnitudes from observed  $V$  magnitudes of flux standards according to known spectral type using the model of Koorneef (1983).

We note that the measured counts in the “sky” frames were not always consistent with those in the “object” frames. From examination of the photometric consistency of the data we are led to conclude that any flux measurements have an uncertainty at the level of 10% (except for 3C 380 in which the uncertainty is  $\sim 20\%$ ). Data reduction was carried out using the CGS4DR package at the QMW and Edinburgh Starlink nodes.

Figure 1 shows the observed spectra. The 14 SL sources are presented in RA order. The spectra of 3C 286 and the three serendipitous sources are given at the end. Note that there are only three SL sources where  $H\alpha$  was not detected. These are 3C 216, 4C 29.45, and 4C 56.27. In a further two sources,  $H\alpha$  is detected but is rather weak (3C 279 and B2 1308+32). In the remaining 9 a strong line was detected. Together with the 8 additional published sources that we use, this produces three sub-samples that we refer to : SL sources ( 22 objects), a sample of 19 SL sources with detected  $H\alpha$  emission, and a sample of 16 strong-EW sources.

### 4.2 Emission line parameters

Emission line measurements were performed using the *DIPSO* package on the ROE Starlink node. In Table 4 we present the observed  $H\alpha$  flux, rest frame EW and FWHM of the flux calibrated spectra. From these data both line and continuum luminosities ( $L_{H\alpha}$  and  $L_o$ ) can be derived. The largest source of error comes from uncertainties in setting the local continuum (fitted by a first order polynomial). To minimize these errors each line was measured on at least three different occasions. In most cases the uncertainties are less than 10%. Experimentation with deblending the narrow lines ( $H\alpha$ , [NII], [SII]) suggests that in most objects its presence does not introduce more than a 3% error into the flux of  $H\alpha$ . This maybe due to our inability to resolve and exclude the narrow lines from either sides of  $H\alpha$ . When the narrow  $H\alpha$  emission line is visible however, its contribution can change substantially FWHM. In these cases the measurements are corrected from narrow line contribution.

In addition to our new data, Table 5 gives the  $H\alpha$  emission line parameters of 8 SL sources with published  $H\alpha$  spectra. These data are less homogeneous than the *UKIRT* spectra. We have searched for total line fluxes and EW (including also NLR), but corrected FWHM (from NLR) values (references are given in Table 5).

## 5 COMMENTS ON INDIVIDUAL OBJECTS

DA 193. The measured line flux and rest EW of the H $\beta$  emission line in this source are  $1.7 \cdot 10^{-14}$  erg cm $^{-2}$  s $^{-1}$  and 40 Å respectively. The total [OIII] flux is estimated as  $9 \cdot 10^{-15}$  erg cm $^{-2}$  s $^{-1}$ . The two spectra obtained of this source show an increase of the continuum flux at shorter wavelengths.

4C 39.25. In the field of 4C 39.25 we have detected what appears to be an extended object (it occupies two detector rows) about 12 arcsec west of our source. We can identify this in the Schmidt plate as a point source which is brighter in the blue. From this and the spectrum (shown in Fig. 1) we conclude that it is a high redshift galaxy.

3C 279. The broad feature at  $1.1 \mu$  of the spectrum is most likely due to the non-fully corrected absorption feature of the spectral standard.

3C 334. The high resolution spectrum obtained in this source (see Fig 1) shows a structured H $\alpha$  emission line profile but it has also a low signal-to-noise ratio. It is also likely not resolved in the continuum, and is arbitrarily multiplied in flux for comparison with the lower resolution H $\alpha$  spectrum.

3C 395. Two other objects, most likely stars, were detected in the slit at 3" east and at 15" west of the source. Their spectra are shown in Fig. 1.

## 6 STATISTICAL RESULTS

We have applied the Spearman rank correlation test (Press *et al.* 1988) to a set of nine parameters - to three emission line parameters (FWHM, EW, and  $L_{H\alpha}$ ), to the optical luminosity at the H $\alpha$  wavelength ( $L_o$ ), to three orientation indicators ( $R$ ,  $\beta_a$  and  $\delta$ ), to  $\theta$ , and finally, to the Lorentz factor,  $\gamma$ . The resulting matrix of the correlation coefficient  $r_s$ , and the two sided significance level of its deviation from zero,  $p$ , is shown in Table 6. The test was applied both to the sub-sample with detected H $\alpha$  lines (N=19) and to the subsample with strong lines, divided at  $EW \geq 158 \text{ \AA}$  (N=16).

The strongest trend is seen between the H $\alpha$  line and continuum luminosity ( $L_{H\alpha}$  and  $L_o$  respectively), especially when only the strong-EW sources are considered. This is however a selection effect, the result of plotting two quantities both multiplied by the same function of redshift. This trend is shown in Fig 2a where the three classes of objects CDP, CD, and LD are shown with separate symbols. (The three objects with H $\alpha$  upper limits are also shown here). The strong- and weak-EW objects are very clearly distinct (see Fig 2b). The weak-EW objects have an EW at least a factor five less than the weakest strong-EW object. Note that the range of luminosities  $L_{H\alpha}$  is not very different in the strong- and weak-EW objects. As we shall see below, the FWHM does not show any such clear discontinuity, so that the two distinct trends in Fig 2 is almost certainly due to a difference in the continuum, not in the line. It is also

striking that all the weak-EW objects are polarised. It seems then extremely likely that the weak-EW objects have a continuum enhanced by relativistic beaming. Very likely there are two continuum components, the first of which is weak in the strong-EW objects, but is boosted to dominance in the weak-EW objects. The object 3C 345 with the largest EW amongst the CDP objects, looks like a good intermediate case, with significant but not dominant relativistic beaming. Broad band polarization and flux density spectra for this object do show the presence of two emission components (Wills 1991): one polarized, likely synchrotron jet radiation, and a second unpolarized possibly from a disc. Optical and Near-IR polarimetric and photometric monitoring also support the two continuum emission components in this source (Smith *et al.* 1986).

In all our subsequent plots, we reclassify objects as simply strong-EW or weak-EW. The weak-EW class is identical with the CDP class except for 3C 345, which has been classed as strong-EW. Within the strong-EW objects, we maintain a distinction between LD and CD objects.

Equivalent width EW is correlated with the various orientation indicators, as indicated in Table 6 and Fig. 3, which collects these correlations graphically. (Note the inverted abscissa for the graphs versus  $\delta$ ,  $R$ , and  $\beta_a$ , chosen so that these can be easily compared with the correlation with  $\theta$ .) Amongst the strong-EW objects, the strongest correlations are with  $\delta$  and with  $\theta$ , in that order. The excellent correlation with  $\delta$  is as expected, as this indicates the amount of Doppler beaming. The fact that it is significantly better, with much less scatter, than the correlation with the indirect orientation indicator  $R$ , indicates that despite the uncertainties, stressed in Section 2, the derived values of  $\delta$  must be quite close to the correct values. The correlation with  $R$  is striking in a special respect as  $R$  is a kind of direct analogue of EW. While EW changes by only a factor of a few,  $R$  changes by a factor of several hundred. There is an anisotropy connected with the radio beaming, but it cannot be the same jet beaming effect (at least for the LD objects), but rather a second "weak beaming" effect. There is a very strong positive correlation between the line EW and the outflow angle of the radio jet in the whole sample, but this is dominated by the cliff at small angles where the jet beaming sets in. The trend slightly weakens in the strong-EW sources and indicates grossly an increase of the EW by a factor of  $\sim 3$  when the viewing angle turns from 5 to 40 degrees.

Next we look at the correlations of FWHM, which are collected in Fig 4. FWHM is correlated with all the orientation indicators, indicating a decrease of the emission line velocity field with increasing beaming. The direct correlation with  $\theta$  is suggestive of axisymmetric motions for the BLR. The most significant correlation seen is with viewing angle  $\theta$ , as shown in Table 6. This is an indication that in deriving  $\theta$  we have done something meaningful. As further support for the reality of the  $\theta$  correlation, note that Table 6 shows no correlation between FWHM and the jet Lorentz factor  $\gamma$ . The weak-EW objects fit well into the same trend as the strong-EW objects, being simply at one end of the trend, namely at small viewing angle. The trends weaken

somewhat when considering the strong-EW sample, which is however in a reduced range of  $\theta$ .

## 7 DISCUSSION

Our main aim has been to compare H $\alpha$  emission properties with observer viewing angle. The most exciting result is that both velocity and equivalent width do indeed correlate with orientation. The actual  $\theta$  derived from the SL motion plus Inverse Compton limit seems more reliable than the various indirect orientation indicators, as it gives stronger trends, and is physical.

The FWHM vs  $\theta$  correlation is suggestive of a flattened structure for the line emitting material. Fig 5a tests this quantitatively, plotting  $V = V_0 \sin \theta$  with normalised line velocity of  $V_0 = 13,000 \text{ km s}^{-1}$  at  $\theta=90^\circ$ . This is the disc fit of Wills & Browne 1986 to the H $\beta$  in a larger AGN sample, extended to larger jet viewing angles. The figure also shows the effect of an isotropic component with  $V = 2,000 \text{ km s}^{-1}$  (see for instance Brotherton *et al.* 1994, Corbin 1997) added in quadrature to the axisymmetric component. The agreement is good. The scatter is considerable, but we should certainly of course expect some dispersion in  $V_0$ . How sensitive is this agreement with the predictions of an axisymmetric structure to the possible errors in  $\theta$ ? As described in section 2, the value of  $\theta$  is strictly an upper limit, as the derived value of  $\delta$  is a lower limit. However, as argued there,  $\delta$  is very insensitive to the true Inverse Compton flux, and the correlations discussed in the previous section confirm that  $\delta$  is unlikely to be in error by more than a factor of a few. We illustrate this sensitivity in Fig 6a by deriving the  $\theta$  values for each source with  $\delta$  increased by a factor three. It can be seen that the effect is still clear but the quantitative fit is not as good. It is also possible that the bulk speed is smaller than the pattern speed responsible for observed SL velocity. We do not illustrate the effect of this explicitly, but note that the net effect is similar to the  $\delta$  effect shown here.

An important implication of a flattened structure for the broad line emitting region (BLR) concerns the mass  $M$ , of the black hole when this is determined from the line velocity width assuming gravitational dynamics and isotropically-oriented motions (e.g. Wandel, Peterson & Malkan 1999, Kaspi *et al.* 2000). In a thin Keplerian BLR of inclination angle equal to  $\theta$  the mass fit of a given line width is  $\propto (\sin^2 \theta \sqrt{\cos \theta})^{-1}$  which is  $\sim 1/\sin^2 \theta$  at low  $\theta$  (Rokaki & Boisson, 1999). The inclination therefore may cause a systematic underestimate of  $M$ , theoretically up to infinity. In more realistic orbital shape of the BLR, involving an aspect ratio of its flattening, the inclination may cause a systematic underestimate of mass by a factor up to  $\sim 100$  (Krolik 2001). It is statistically implausible that the mass of the quasars is underestimated by such a large factor (this would happen if all sources are observed with  $\theta=0$ ) but it could be important for sources found accreting at super-Eddington rates (see Collin *et al.* 2002). The FWHM vs  $\theta$  correlation therefore, supports estimates of the black hole mass in which

an orientation dependence of the line width is applied (e.g. Lacy *et al.* 2001, McLury & Dunlop 2002).

The EW correlation shows the presence of two separate beaming effects - a strong effect presumably connected with relativistic beaming in the jet, and a second weaker effect, producing a factor  $\sim 3$  change for  $\theta$  range from 5 to 40 degrees. It is tempting to identify this second effect with the  $\cos \theta$  surface brightness effect expected from a flat accretion disc. Fig 5b examines this possibility quantitatively. The dot-dashed curve shows the expected effect of Doppler enhancement for a jet with  $\gamma = 30$  (imposed mainly from the objects with large  $\beta_a$ ). This can explain the difference between CDP objects and the rest, but not the general trend. The dotted line combines an isotropic continuum with a second separate jet-beamed continuum. This also does not fit the overall pattern. The dashed line shows the predicted effect for a flat accretion disc, with standard limb darkening, where we should find  $EW = EW_0 [1/3 \cos \theta (1 + 2 \cos \theta)]^{-1}$ . Fig 5b plots this with  $EW_0 = 300 \text{ \AA}$ . Note that apart from the normalisation there is no further degree of freedom. The solid line combines this disc-beamed continuum with a second separate jet-beamed continuum. The overall fit is good.

In Fig 6b, we indicate the effect on  $\theta$  of changing  $\delta$  by a factor of three, as explained in the FWHM discussion. The qualitative trend is still clear, but the quantitative fit is not as good. Given this uncertainty, we cannot hope, for example, to distinguish classes of accretion disc models such as flat discs, thick discs and flared discs. It is possible to restrict the range of  $\theta$  in the sample (e.g. by decreasing  $H_o$ ), more than in Fig 6b. In this case a jet model with a broad distribution of  $\gamma$  could possibly account for the observed correlation, but requiring small  $\gamma$  ( $<5$ ) for lobe dominated objects (not seen in Table 2).

Another worry is that we have implicitly assumed that the continuum light has a surface brightness effect with  $\theta$ , but that the line emission does not. If the BLR is however axisymmetric, as the FWHM effect seems to show, then H $\alpha$  emission may come from the surface of the disc, and suffer a very similar effect with  $\theta$ , removing the EW vs  $\theta$  effect. The effect would be the same as the dotted line in Fig 5b, showing isotropic continuum, which clearly does not fit the data. However, a likely scenario is that the line emitting material is in an axisymmetric structure but is *not* from the surface of an optically thick disc, being rather in a flattened system of clouds. Even if the lines are emitted from the surface of a disc, they will not necessarily suffer the same limb darkening law.

If the observed optical continuum of the strong line class is emitted from a disc, it is not likely that it is markedly influenced by relativistic effects such as the gravitational redshift and lensing. These effects are stronger when the disc is viewed in the equatorial plane (and in the Kerr metric, Cunningham 1975), which is not the case for the SL objects.

## 8 CONCLUSIONS

In this paper we have investigated the relation of the H $\alpha$  emission line with radio beaming and outflow angle in a sample of SL sources. Most of the H $\alpha$  spectra were observed by us at the *UKIRT* and are reported here.

The sample is divided into two classes: 6 weak-EW and 16 strong-EW quasars. The weak-EW class must have a relativistically beamed continuum, since it has also high radio core dominance and high optical polarization. The strong-EW class shows a clear beaming effect, but one that cannot be relativistic beaming alone, since the line EW changes only by a factor of a few. The correlation with the actual viewing angle derived from the superluminal motions is very clear and nicely consistent with this weak beaming being due to the surface brightness effect expected from tilting a flat accretion disc. We also find that the FWHM of H $\alpha$  is correlated with the viewing angle in a manner quantitatively consistent with the idea that the line emitting material is an axisymmetric rotating structure. However, the line emission cannot come from the surface of an optically thick disc, otherwise the line beaming would cancel the continuum beaming. Overall it seems most likely that the optical continuum comes from a flat accretion disc whereas the line emission is from an axisymmetric system of clouds.

## ACKNOWLEDGMENTS

We are grateful to the *UKIRT* team for their help in the observations. We thank Suzy Collin for helpful discussion, and Anne-Marie Dumont, Catherine Boisson and Maria Kontizas for help in this work. We also thank the referee, Bev Wills, for critical comments which improved this work. ER acknowledges a UK PPARC and a Greek IKY fellowship.

## REFERENCES

- Alberdi A., Krichbaum T.P., Graham D.A. *et al.* 1997, *A&A* 327, 513  
Alef W., Wu S.Y., Preuss E., Kellermann K.I., Qiu Y. H., 1996 *A&A* 308, 376  
Antonucci R.R.J., 1993. *AnnRev A&A* 31 473  
Antonucci R.R.J., Miller J.S., 1985, *ApJ*, 297, 621  
Bloom S.D., Marscher A.P., 1991, *ApJ* 366, 16  
Brinkmann W., Siebert J., Reich W., *et al.* , 1995, *A&ASS* 109, 147  
Brinkmann W., Yuan W., Siebert J., 1997, *A&A* 319, 413  
Brotherton M.S., Wills B.J., Steidel C.C., Sargent W.L.W., 1994, *ApJ* 423, 131  
Browne I.W.A., Murphy D.W., 1987, *MNRAS* 226, 601.  
Brunthaler A., Falcke H., Bower G.C., *et al.* , 2000, *A&A* 357, L15  
Charlot P., 1990, *A&A*, 229, 51  
Collin-Souffrin S., 1987, *A&A* 179, 60  
Collin S., Boisson C., Mouchet M., Dumont A.M., Coupe S., *et al.* 2002, *A&A* 388, 771  
Corbett E.A., Robinson A., Axon D.J., Hough J.H., Jeffries R.D., *et al.* , 1996, *MNRAS* 281, 737  
Corbin M.R., 1997, *ApJS* 113, 245  
Cunningham C., 1975, *ApJ* 202, 788  
Eracleous M., Halpern J.P., 1994, *ApJS* 90, 1  
Freedman W.L., *et al.* , 2001, *ApJ* 553, 47.  
Gabuzda D.C., Kollgaard R.I., Roberts D.H., Wardle J.F.C., 1993, *ApJ* 410, 39  
Gabuzda D.C., Mullan C.M., Cawthorne T.V., Wardle J.F.C., Roberts D.H., 1994, *ApJ* 435, 140  
Ghisellini G., Padovani P., Celotti A., Maraschi L., 1993, *ApJ*, 407, 65  
Hooimeyer J.R.A., Barthel P.D., Schilizzi R.T., Miley G.K., 1992, *A&A* 261, 1 (H1)  
Hooimeyer J.R.A., Schilizzi R.T., Miley G.K. & Barthel P.D. 1992, *A&A* 261, 5 (H2)  
Hough D.H., Readhead A.C.S., 1987, *ApJ* 321, L11  
Hough D.H., Readhead A.C.S., Wood D.A., Jr., Feldmeier J.J., 1992, *ApJ* 393, 81  
Jackson N., Browne I.W.A., Murphy D.W., Saikia D.J., 1989, *Nature* 338, 485.  
Jackson N., Browne I.W.A., 1991a, *MNRAS* 250, 414  
Jackson N., Browne I.W.A., 1991b, *MNRAS* 250, 422  
Kaspi S., Smith P.S., Netzer H., Maoz D., Jannuzi B.T., Giveon U., 2000, *ApJ* 533, 631  
Koorneef J., 1983, *A&A*, 128, 84  
Krolik J., 2001, *ApJ* 551, 72 2001ApJ...551L..17L 1.000 04/2001 A E F R C S U  
Lacy M., Laurent-Muehleisen S.A., Ridgway S.E., Becker R.H., White R. L. 2001, *ApJ* 551, L17  
Lara L., Alberdi A., Marcaide J.M., Muxlow T.W.B., 1999 *A&A* 352, 443  
Lawrence A., Elvis M., 1982, *ApJ* 256, 410  
Lawrence C.R., Zucker J.R., Readhead A.C.S., Unwin S.C., Pearson T.J., Xu W., 1996, *ApJS* 107, 541  
Ledden J.E., Odell S.L., 1985, *ApJ* 298, 630  
Lightman A.P., Shapiro S.L., 1975, *ApJ* 198, L73  
Lind K.R., Blandford R.D., 1985, *ApJ* 295, 358  
Madau P., Ghisellini G., Persic M., 1987, *MNRAS* 224, 257  
Mantovani F., Junor W., McHardy I.M., Valerio C., 2000, *A&A* 354, 497  
McHardy I.M., Marscher A.P., Gear W.K., Muxlow T., Lehto H.J., Abraham R. G., 1990, *MNRAS* 246, 305  
McLure R.J., Dunlop J.S., 2002, *MNRAS* 331, 795  
Netzer H., 1982, *MNRAS* 198, 589  
Neugebauer G., Oke J.B., Becklin E.E., Matthews K., 1979, *ApJ* 230, 79  
Orr M.J.L., Browne I.W.A., 1982, *MNRAS*, 200, 1067  
Pauliny-Toth I.I.K., Preuss E., Witzel A., Graham D., Kellerman K.I., Ronnang B., 1981, *AJ* 86, 371  
Pearson T.J., Readhead A.C.S., 1988, *ApJ* 328, 114  
Polatidis A.G., Wilkinson P.N., 1998, *MNRAS* 294 327  
Press W.H., Flannery B.P., Teukolsky S.A., Vetterling W.T., *Numerical Recipes*, Cambridge University Press, 1988.  
Rees M.J., 1966, *Nature*, 211, 468  
Rees M.J., 1975, *MNRAS* 171, 457  
Rafanelli P., 1985, *A&A*, 146, 17  
Rokaki E., Boisson C., 1999, *MNRAS*, 307, 41  
Ros E., Zensus J.A., Lobanov A.P., 2000, *A&A* 354, 55  
Soifer B.T., Neugebauer G., Oke J.B., Matthews K., 1981, *ApJ* 243, 369  
Smith P.S., Balonek T.J., Heckert P.A., Elston R., 1986, *ApJ* 305, 484  
Urry C.M., Padovani P., 1995, *PASP* 107, 803  
Vermeulen R.C., Bernstein R.A., Hough D.H., Readhead A.C.S., 1993, *ApJ* 417 541  
Vermeulen R.C., Cohen M.H., 1994, *ApJ*, 430, 467, (VC94)  
Wandel A., Peterson B.M., Malkan M.A., 1999, *ApJ* 526, 579

- Wehrle A.E., Piner B.G., Unwin S.C., Zook A.C., Xu W. *et al.*, 2001, ApJS, 133, 297
- Wills B. J., Browne I. W. A., 1986, ApJ, 302, 56
- Wills B.J., 1991, in *Variability of AGN*, conf. in 1990 Atlanta, Georgia, eds. Miller H.R. & Wiita P.J., p. 87.
- Wills B.J., Wills D., Breger M., Antonucci R.R.J., Barvainis, R. *et al.* 1992, ApJ 398, 454
- Wills, B.J., Brotherton, M.S., 1995, ApJ 448L, 81
- Zensus J. A., Pearson T. J., 1987, in *The impact of VLBI on astrophysics and geophysics*, Proceedings of the 129th IAU Symposium, Cambridge, MA, May 10-15, 1987 (A89-13726 03-90). Dordrecht, Kluwer Academic Publishers, 1988, p. 7-16.

## 9 FIGURE CAPTIONS

**Figure 1** The observed flux calibrated spectra obtained with *CGS4* at *UKIRT*. The 14 SL sources are presented in RA order. The spectra of 3C 286 and the three serendipitous sources are given at the end. Note that there are only three SL sources where  $H\alpha$  was not detected (the expected wavelength is indicated in 3C 216, 4C 29.45, and 4C 56.27).

**Figure 2** (a): The  $H\alpha$  line versus continuum luminosity of the SL sample. (b): The EW versus the continuum luminosity. CDP, CD and LD objects are shown with cross, X and star symbols respectively. Small filled circle symbols show the *UKIRT* data. Upper limits are noted.

**Figure 3** The  $H\alpha$  EW versus  $R$ ,  $\beta_a$ ,  $\delta$ , and  $\theta$ , (in a,b,c and d respectively) of the 22 SL objects. In these and all subsequent figures, circles designate the strong-EW objects (open and filled symbols are core and lobe dominated sources respectively). Note the inverted abscissa for the graphs versus  $\delta$ ,  $R$ , and  $\beta_a$ , chosen so that these can be easily compared with the correlation with  $\theta$ .

**Figure 4** The  $H\alpha$  FWHM versus the orientation indicators as in Fig 3, for the 19 objects with detected line emission.

**Figure 5** (a): FWHM versus  $\theta$  compared with models. The dashed curve shows an axisymmetric component ( $V = 13,000 \sin \theta \text{ km s}^{-1}$ ) and the solid curve gives its quadrature sum with an isotropic one ( $V=2,000 \text{ km s}^{-1}$ , the dotted curve). (b): EW versus  $\theta$  compared with models. Note the inverted EW axis indicating the brightness of the underlying continuum. The dot-dashed curve shows the expected effect of Doppler enhancement for a jet with  $\gamma=30$ . The dashed curve shows the predicted effect for a flat accretion disc with a standard limb darkening, and the solid curve combines disc and beamed component. The dotted curve combines an isotropic and a beamed component.

**Figure 6** Same as Fig 5, but with  $\theta$  recalculated using  $\delta$  bigger by factor three to show sensitivity to errors.

**Figure 1.**

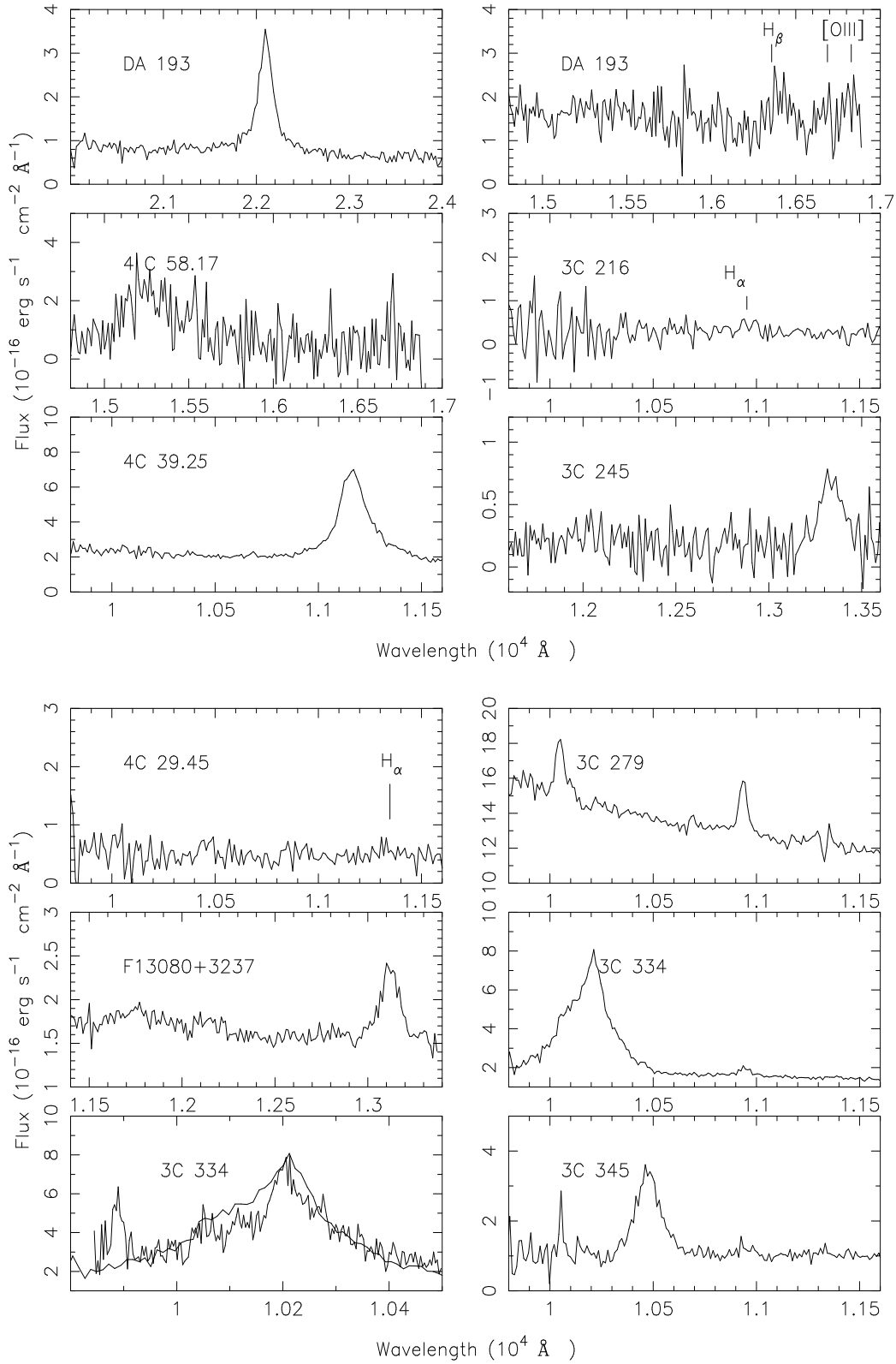


**Figure 1.** - *continued*

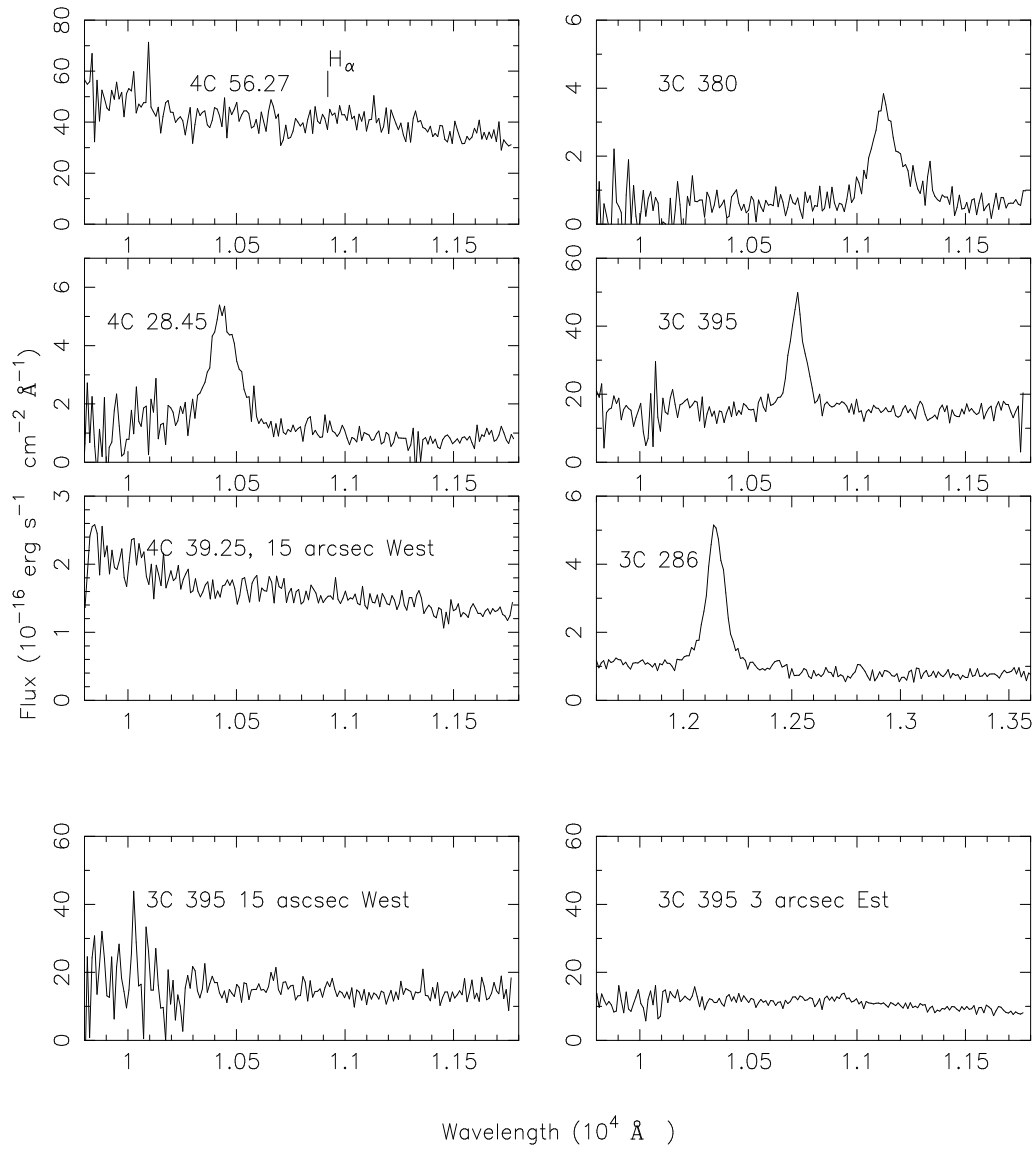


**Table 1.** Names, redshift, SL speed and radio core dominance of the SL sample taken from VC94. The observed radio core flux and angular size at a given wavelength, and the X-ray flux at 1 keV are given together with the references.

IAU name (1)	Common name (2)	Class (3)	z (4)	$\beta_a$ <sup>1</sup> c (5)	log $R$ (6)	$S_\nu$ Jy (7)	$\nu$ GHz (8)	$\theta_d$ mas (9)	Ref. Radio (10)	$F_X$ $\mu$ Jy (11)	Ref. X-ray (12)
0007+106	III Zw 2 <sup>2</sup>	CD	0.089	1.25	>1.44	1.540	43	0.075	B00	2.74	B
0133+207	3C 47	LD	0.425	4.9	-1.30	0.084	10.7	0.15	V93	0.44	B
0430+052	3C 120	CD	0.033	5.4	0.80	3.900	5.0	0.40	P81	10.00	BM
0552+398	DA 193	CD	2.365	2.3	0.60	2.620	8.4	0.73	C90	0.49	B
0850+581	4C 58.17	CD	1.322	5.2	0.27	0.940	5.0	0.48	PR	0.06	B
0906+430	3C 216	CDP	0.669	5.1	-0.01	0.880	5.0	0.10	PR	0.11	B
0923+392	4C 39.25	CD	0.699	5.3	1.30	0.200	22.2	0.05	A97	0.58	B
1040+123	3C 245	CD	1.029	4.1	0.00	0.590	10.7	0.33	HR	0.13	B
1156+295	4C 29.45	CDP	0.729	34.8	0.83	1.400	22.2	0.12	H90	0.18	B
1226+023	3C 273	CD	0.158	10.7	0.90	1.820	22.0	0.21	M00	10.89	B
1253-055	3C 279	CDP	0.538	12.2	1.10	12.310	22.0	0.08	W01	0.96	B
1308+326	B2	CDP	0.996	27.7	1.60	0.540	5.0	0.18	G93	0.13	B
1618+177	3C 334	LD	0.555	2.5	-0.64	0.086	10.7	0.20	H92	0.20	B
1641+399	3C 345	CDP	0.595	12.4	1.50	2.750	22.0	0.13	RO	0.57	B
1721+343	4C 34.47	LD	0.206	3.2	-0.10	0.109	10.7	0.24	H1	2.37	B
1823+568	4C 56.27	CDP	0.664	3.4	2.30	0.728	5.0	0.31	G94	0.36	B95
1828+487	3C 380	CD	0.691	11.1	0.70	1.168	5.0	0.32	PW	0.63	B
1830+285	4C 28.45	LD	0.594	3.4	-0.28	0.303	5.0	0.50	H2	0.31	B
1845+797	3C 390.3 <sup>3</sup>	LD	0.057	2.4	-1.00	0.310	5.0	0.50	LO	1.10	LO
1901+319	3C 395	CD	0.635	17.6	0.50	0.124	4.8	0.06	L99	...	...
1928+738	4C 73.18	CD	0.302	9.4	0.70	2.110	5.0	0.49	PR	1.05	B
2200+420	BL Lac	CDP	0.069	5.0	2.40	1.600	5.0	0.35	M87	0.82	M87

1. Unless otherwise noted  $\beta_a$  is from VC942.  $\beta_a$  and  $R$  from B00 and WB3.  $\beta_a$  and  $R$  from A96 and WB

## REFERENCES:

A96: Alef *et al.* 1996A97: Alberdi *et al.* 1997B: Brinkmann *et al.* 1997B00: Brunthaler *et al.* 2000B95: Brinkmann *et al.* 1995

BM: Bloom &amp; Marscher 1991

C90: Charlot 1990

G93: Gabuzda *et al.* 1993G94: Gabuzda *et al.* 1994H1: Hooimeyer *et al.* 1992H2: Hooimeyer *et al.* 1992H90: McHardy *et al.* 1990H92: Hough *et al.* 1992

HR: Hough &amp; Readhead 1987

L99: Lara *et al.* 1999

LO: Ledden &amp; Odell 1985

M00: Mantovani *et al.* 2000M87: Madau *et al.* 1987P81: Pauliny-Toth *et al.* 1981

PR: Pearson &amp; Readhead 1988

PW: Polatidis &amp; Wilkinson 1998

RO: Ros, Zensus &amp; Lobanov 2000

V93: Vermeulen *et al.* 1993W01: Wehrle *et al.* 2001

WB: Wills &amp; Browne 1986

**Table 2.** The derived  $\delta$ ,  $\gamma$  and  $\theta$  (in degrees) of the SL sources listed in increasing  $\theta$ .

Name	$\delta$	$\gamma$	$\theta^\circ$
3C 279	73.45	37.75	0.25
3C 216	42.58	21.61	0.32
4C 29.45	6.22	100.55	3.19
1308+326	11.59	38.94	3.52
3C 395	5.07	33.26	6.00
3C 345	8.45	13.33	6.32
3C 380	6.22	13.09	7.86
4C 73.18	3.92	13.29	10.39
3C 273	1.07	54.94	10.55
4C 58.17	5.42	5.31	10.62
3C 120	5.32	5.51	10.82
4C 56.27	4.45	3.64	12.64
BL Lac	4.43	5.12	12.92
DA 193	3.76	2.72	13.99
4C 39.25	2.64	6.83	17.31
III Zw 2	2.43	1.74	21.11
3C 47	0.50	25.37	22.75
3C 245	1.73	6.12	23.41
4C 28.45	0.83	8.02	31.01
4C 34.47	0.19	29.24	35.05
3C 334	0.40	9.19	42.68
3C 390.3	0.45	7.85	43.76

**Table 3.** The *UKIRT* observing log. Unless otherwise noted, the observations were made in *J* band.

Name	Obs. date	Seeing arcsec	Exp. time min	Notes
DA 193	29/3/94	1.16	46	<i>K</i> , grating in first order
	29/3/94	1.35	72	<i>H</i> , 600 km s <sup>-1</sup>
4C 58.17	29/3/94	1.32	55	<i>H</i> , 600 km s <sup>-1</sup>
3C 216	29/3/94	1.31	27	
4C 39.25	27/3/94	1.07	60	2 objects in the slit
3C 245	28/3/94	1.10	80	
4C 29.45	28/3/94	1.04	35	
3C 279	27/3/94	1.23	88	
1308+326	27/3/94	1.02	86	
3C 286	29/3/94	1.06	75	z=0.849
3C 334	27/3/94	1.04	60	
	28/3/94	1.30	85	150 l/mm, R=1000
3C 345	27/3/94	1.08	60	
4C 56.27	29/3/94	1.38	30	
3C 380	28/3/94	1.27	40	
4C 28.45	28/3/94	1.06	15	
3C 395	29/3/94	1.15	30	3 objects in the slit

**Table 4.** The observed H $\alpha$  flux (in  $10^{-14}$  erg cm $^{-2}$  s $^{-1}$ ), rest frame EW and FWHM of the *UKIRT* H $\alpha$  spectra.

Name	Flux	EW Å	FWHM Km s $^{-1}$
DA 193	6.00	240	2450
4C 58.17	3.40	240	4100
3C 216	<0.05	<10	
4C 39.25	8.60	295	4000
3C 245	0.84	316	3250
4C 29.45	<0.06	<8	
3C 279	1.40	8	1400
1308+326	0.90	30	2350
3C 286	4.6	254	2600
3C 334	13.60	446	6150
3C 345	3.25	186	3600
4C 56.27	<1.33	<2	
3C 380	3.37	380	3500
4C 28.45	6.67	354	4050
3C 395	28.60	158	2050

**Table 5.** The observed H $\alpha$  flux (in  $10^{-14}$  erg cm $^{-2}$  s $^{-1}$ ), rest frame EW and FWHM and the references to the published H $\alpha$  spectra.

Name	Flux	EW Å	FWHM Km s $^{-1}$	Ref.
III Zw 2	136	445	3600	N79,R85
3C 47	10.5	392	8400	JB
3C 120	77.0	299	1846	RB
3C 273	650.0	369	3260	JB
4C 34.47	65.0	589	2300	S81, EH
3C 390.3	80.6	519	11900	N82,L96,EH
4C 73.18	38.0	365	3100	JB,EH
BL Lac	28.7	7.3	4000	C96

## REFERENCES:

C96: Corbett *et al.* 1996, EH: Eracleous & Halpern 1994  
 JB: Jackson & Browne 1991a, measured in scanned spectra  
 L96: Lawrence *et al.* 1996, N82: Netzer 1982  
 N79: Neugebauer *et al.* 1979, R85: Rafanelli 1985  
 RB: Rokaki & Boisson 1999, S81: Soifer *et al.* 1981

**Table 6.** The matrix of the correlation coefficient  $r_s$ , and the two sided significance level of its deviation from zero,  $p$ , for the sub-sample with detected H $\alpha$  lines (N=19) and for the subsample with strong lines (N=16). Correlations with  $p < 0.02$  are shown in bold type.

	FWHM		EW		$L_o$		$L_{H\alpha}$	
	$r_S$	$p$	$r_S$	$p$	$r_S$	$p$	$r_S$	$p$
Strong- and weak-EW objects, N=19								
EW	0.37	0.115						
$L_o$	-0.28	0.244	-0.42	0.074				
$L_{H\alpha}$	0.02	0.949	0.10	0.687	<b>0.71</b>	<b>0.001</b>		
$R$	-0.38	0.107	<b>-0.62</b>	<b>0.005</b>	0.08	0.744	-0.29	0.228
$\beta_a$	-0.46	0.047	<b>-0.59</b>	<b>0.008</b>	0.37	0.115	-0.01	0.983
$\delta$	-0.47	0.043	<b>-0.78</b>	<b><math>7.5 \cdot 10^{-5}</math></b>	0.28	0.241	-0.22	0.363
$\gamma$	-0.32	0.178	-0.02	0.930	0.42	0.075	0.17	0.477
$\theta$	<b>0.57</b>	<b>0.011</b>	<b>0.70</b>	<b>0.001</b>	-0.49	0.033	-0.01	0.955
Strong-EW objects, N=16								
EW	0.33	0.214						
$L_o$	-0.07	0.805	-0.52	0.040				
$L_{H\alpha}$	-0.14	0.615	-0.34	0.192	<b>0.96</b>	<b><math>5 \cdot 10^{-9}</math></b>		
$R$	-0.41	0.113	-0.44	0.092	0.09	0.747	0.01	0.976
$\beta_a$	-0.33	0.215	-0.52	0.037	0.25	0.345	0.15	0.572
$\delta$	-0.33	0.207	<b>-0.74</b>	<b>0.001</b>	0.17	0.535	0.01	0.983
$\gamma$	-0.11	0.674	0.13	0.623	0.22	0.412	0.26	0.333
$\theta$	0.46	0.076	<b>0.67</b>	<b>0.005</b>	-0.40	0.122	-0.28	0.289

**Figure 2.**

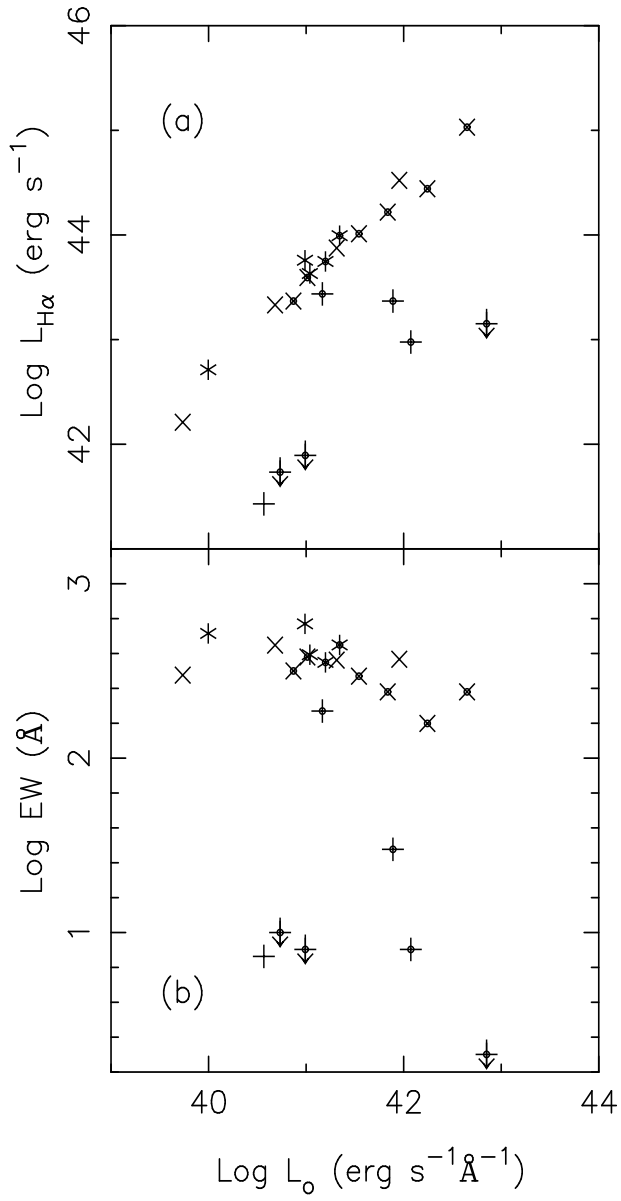


**Figure 3.**

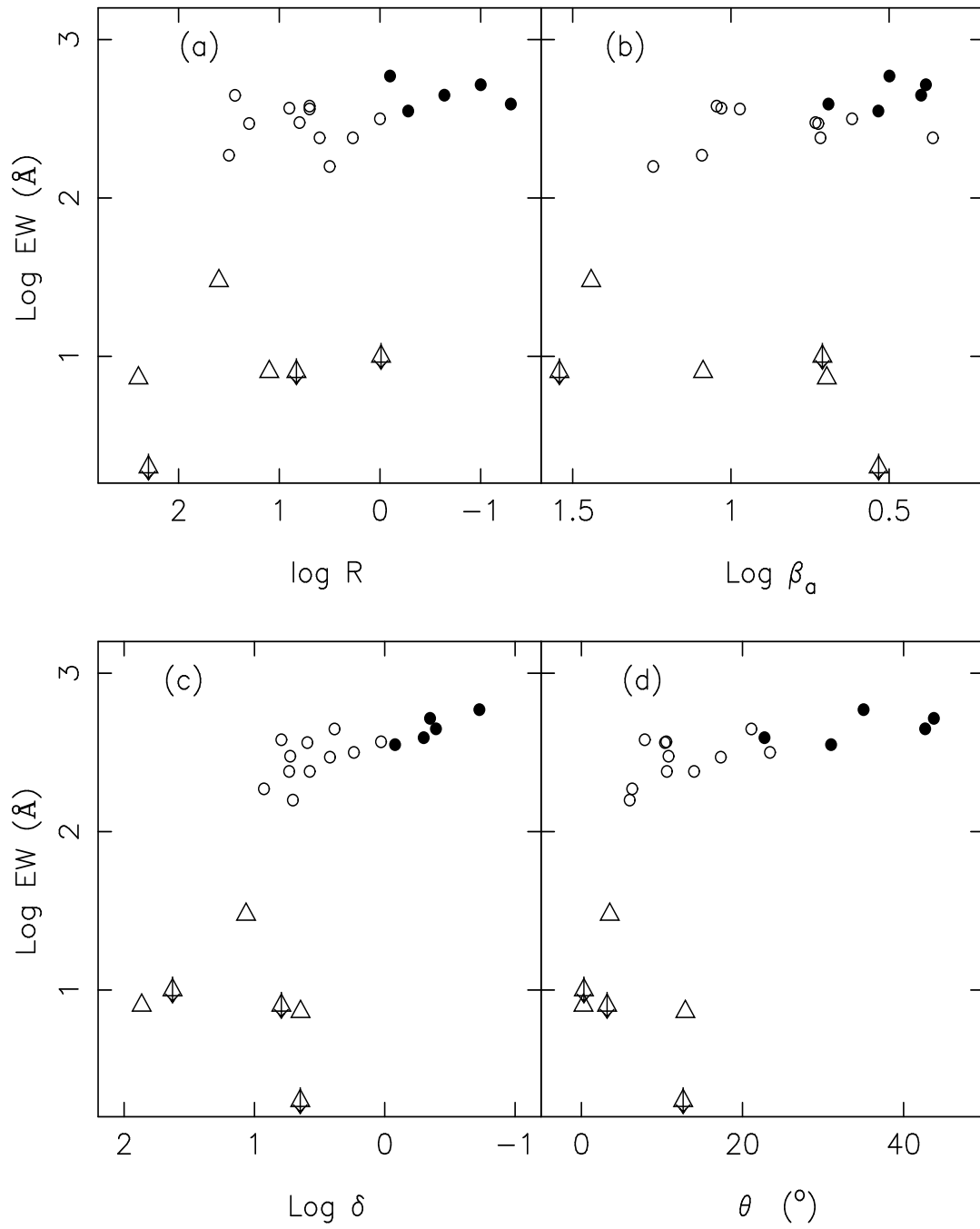


**Figure 4.**

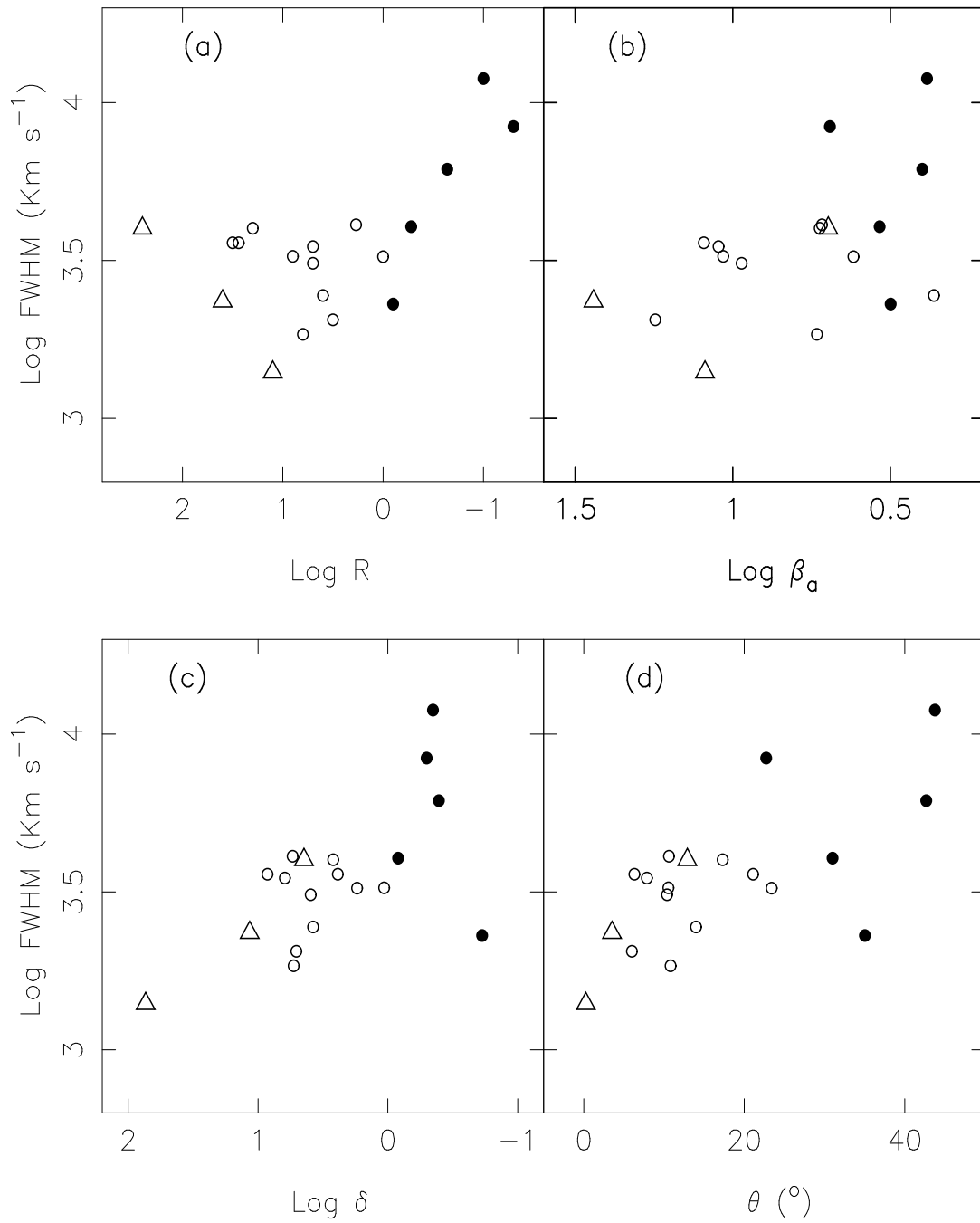


**Figure 5.**

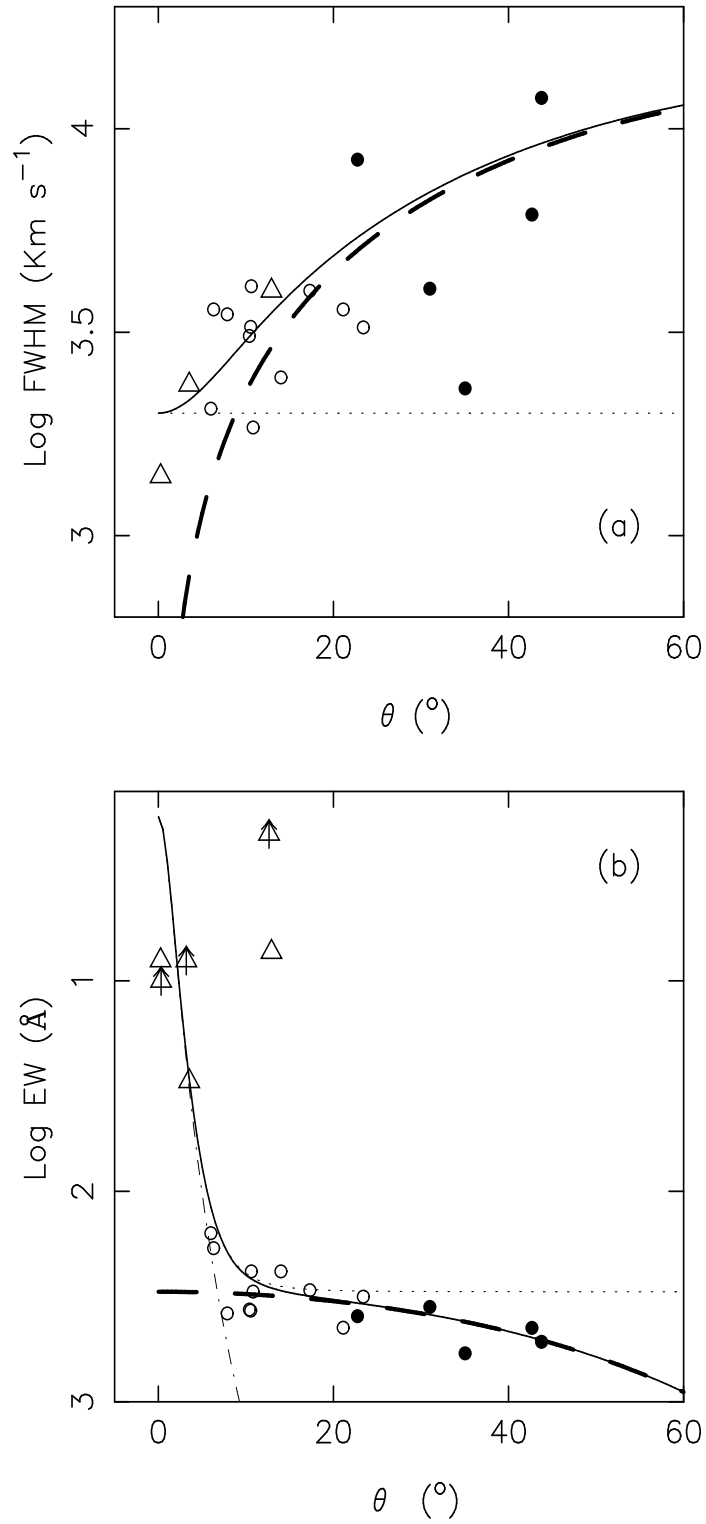


**Figure 6.**

